Impact of interfacial curvature on molecular properties of aqueous interfaces

M. de la Puente, D. Laage

Impact of Interfacial Curvature on Molecular Properties of Aqueous Interfaces

M. de la Puente[1] and D. Laage[1]

PASTEUR, Department of Chemistry, École Normale Supérieure,

PSL University, Sorbonne Université, CNRS, 75005 Paris,

France

(*Electronic mail: damien.laage@ens.psl.eu)

(Dated: 20 May 2024)

The curvature of soft interfaces plays a crucial role in determining their mechanical and thermodynamic properties, both at macroscopic and microscopic scales. In the case of air/water interfaces, a particular attention has recently focused on water microdroplets, due to their distinctive chemical reactivity. However, the specific impact of curvature on the molecular properties of interfacial water and on interfacial reactivity has so far remained elusive. Here we use molecular dynamics simulations to determine the effect of curvature on a broad range of structural, dynamical and thermodynamical properties of the interface. For a droplet, a flat interface and a cavity, we successively examine the structure of the hydrogen-bond network and its relation to vibrational spectroscopy, the dynamics of water translation, rotation and hydrogen-bond exchanges, and the thermodynamics of ion solvation and ion-pair dissociation. Our simulations show that curvature predominantly impacts the hydrogen-bond structure through the fraction of dangling OH groups, and the dynamics of interfacial water molecules. In contrast, curvature has a limited effect on solvation and ion-pair dissociation thermodynamics. For water microdroplets, this suggests that the curvature alone cannot fully account for the distinctive reactivity measured in these systems of great importance for catalysis and atmospheric chemistry.

I. INTRODUCTION

Water is an intriguing liquid, because of its fascinating anomalies in bulk solution of course, but also because of its puzzling properties when in confined geometries such as droplets and nanochannels. While confined water systems have been used to indirectly investigate the bulk properties, offering the ability to manipulate thermodynamic anomalies[1] like shifting the homogeneous nucleation temperature and the liquid-liquid phase transition,[2] they are garnering increasing interest for their own distinct properties and their significance, particularly in atmospheric aerosols,[3] catalysis[4] and microfluidics.[5]

The study of chemical reactivity at aqueous interfaces has grown exponentially in the last decades.[3] Between the discovery of "on-water" catalyzed reactions[6] almost twenty years ago and the now thriving field of "on-droplet" catalysis,[7] a great variety of organic[4] and inorganic[8] reactions have been found to proceed differently at soft water interfaces compared to the bulk. A number of suggestions have been made to explain the distinct reactivity in droplets, invoking, *e.g.*, different solvation properties in the bulk and at the interface,[9–11] the surface activity of the products,[12] reactant accumulation and increased rate constant at the interface,[13] and strong electric fields at the water surface.[14–16] In addition to these effects, the interfacial curvature of water microdroplets has also been proposed (see, *e.g.*, refs 17,18) to be a critical factor determining their unique features. Curvature is expected to impact a range of physical and chemical properties at interfaces. First, curvature is known to affect the water surface tension.[19] Second, curvature determines the Laplace pressure which has been suggested to induce distinct chemical reaction kinetics in nanometric atmospheric aerosols.[17,18] Third, curvature-related capillary effects are known to modify chemical equilibria at the mesoscopic scale.[20,21] In addition, for hydrophobic solutes, the solute size which determines the curvature of its interface with water has been proposed to be a key factor governing the solute hydration thermodynamics.[22,23] Finally, curvature has recently been suggested to modify the strength of the water hydrogen-bond (H-bond) network: vibrational spectroscopy measurements reported that whereas at a flat air-water interface H-bonds are slightly weaker than in the bulk,[24] they become stronger than in the bulk at the curved interfaces of a sub μm-scale oil droplet in water[25] and of a sub μm-scale water droplet in oil.[26]

However, despite the suggested importance of curvature in interfacial reactivity, a detailed molecular characterization of the curvature's impact on the interfacial properties of water is still lacking. Experimental investigations face a number of challenges, including, *e.g.*, the difficulty

to obtain a monodisperse assembly of systems with the same curvature since broad size distributions are typically found in emulsions and aerosols, and the difficulty to systematically vary the curvature without affecting any other parameter of the system. Molecular dynamics (MD) simulations therefore appear as a well-suited tool to gain a molecular-level description of the changes specifically induced by curvature on the properties of interfacial water.

We report here the results of MD simulations of a series of systems with water interfaces of different curvatures, and we characterize a broad range of molecular properties at these interfaces. The remainder of this article is structured as follows. First, we describe our simulation methodology and our simulated systems, which include a sub-nm water droplet (positive curvature), a water solution in contact with a sub-nm hydrophobic cavity (negative curvature), a flat liquid water slab (zero curvature), and ions solvated in droplets. We then characterize the structure of the interface, focussing on the H-bond network configuration and its relation to vibrational spectra. We further determine the dynamics of water molecules at the interface, including their translational, reorientational and H-bond exchange dynamics. We then study the hydration free energies of fluoride and iodide ions at these different interfaces and calculate the dissociation thermodynamics of a sodium fluoride ion pair in droplets of increasing curvature. We finally provide some concluding remarks regarding the impact of curvature on interfacial water properties.

II. METHODS

A. Simulated Systems

We have simulated systems presenting three types of curvatures: droplets (whose curvature we define as positive), cavities (negative curvature) and slabs (zero curvature), with the curvature κ defined as the inverse of the radius of curvature R for each system. For our study of the structural and dynamical properties of the air/water interface, we have considered the following three systems (see Fig. 1): a 7.5 Å radius droplet of 128 water molecules within a cubic (64 Å)^3 box, a 7.3 Å radius spherical cavity created by a Lennard-Jones sphere within a solution of 800 water molecules in a 3D periodic cubic box of (29.5 Å)^3 (mimicking an oil nanodroplet), and a slab system of 903 water molecules in a rectangular box of 30 Å along the x and y directions and 120 Å along the z direction, leaving a vapor gap approximately three times thicker than the water film. These systems will be identified as the default *droplet, cavity* and *slab* systems.

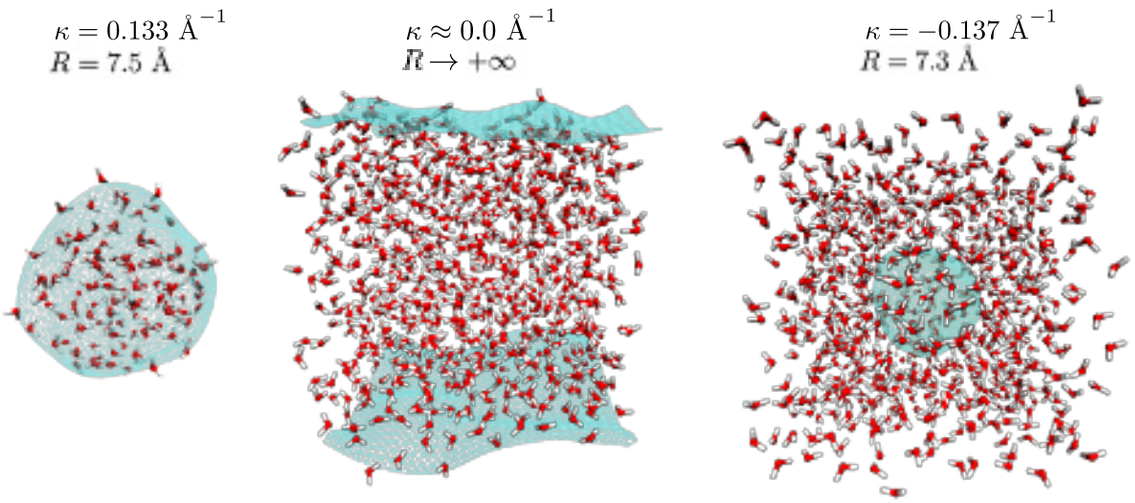

FIG. 1. From left to right: droplet, slab and cavity simulation systems and associated curvature κ and radius R. Blue mesh-grids represent the instantaneous air-water interface.[27]

In our simulations, while the droplet and the slab correspond to a liquid/vapor interface, the cavity system simulates an interface between water and an apolar solute. This is because a vapor bubble is not stable under ambient conditions. Applying negative pressure would stabilize this cavity[28] but it would also affect the dynamics of water,[29] making it ambiguous to disentangle the effects of curvature and pressure when compared with the droplet and slab systems. We therefore retain the ambient conditions for our simulation, but introduce a spherical Lennard-Jones solute to maintain the cavity. Although on a different scale, this is analogous to experiments performed on oil nanodroplets in water.[25] Although this Lennard-Jones potential affects, *e.g.*, the interfacial capillary fluctuations, it remains weak and acts only on the oxygen atoms (see section II.B). Therefore, it is expected to have a very limited effect on the H-bond arrangement of the interfacial molecules. As will be shown below, it is this H-bond arrangement that determines the structural, dynamic and spectroscopic properties of the water interface measured in this study. Therefore, we expect that the difference in interfacial properties reported for the three systems is essentially due to curvature effects and not to the interactions of water with the apolar solute.

To study ion solvation, the corresponding ion (fluoride or iodide) was directly added into the system without changing the geometry or constraints in place. To determine the ion pair dissociation thermodynamics, we compared two droplets of different sizes and two bulk solutions whose

salt concentrations are equal to these in the droplets. We have considered two systems of 256 and 512 water molecules and a sodium fluoride pair in (64 Å)^3 cubic boxes, which formed droplets with curvature radii of 11.6 Å and 14.9 Å respectively (see inset in Fig. 11). In order to account for concentration effects, we considered the same ion pair dissociation in bulk systems with 256 and 512 water molecules in 3D-periodic cubic boxes of (19.6 Å)^3 and (24.7 Å)^3 respectively.

B. Molecular Dynamics Simulations

Water was described with the well-established SPC/E model,[30] which has been shown to correctly reproduce the water surface tension,[31] the air-water interface vibrational sum-frequency generation spectrum,[32,33] bulk water dynamics,[34] and the IR and Raman spectra of bulk water.[35] This model should therefore give a correct description of both bulk and interfacial water properties. Ions were described by the Joung and Cheatham potential for combination with SPC/E water.[36] The cavity was created by inserting a 6 Å-radius sphere interacting with water via a Lennard-Jones potential ($\varepsilon = 0.069$ kcal·mol^{-1}, $\sigma = 3.390$ Å) applied to the distance to the sphere surface. All simulations were propagated with LAMMPS[37,38] in the canonical ensemble at 300 K, with a velocity rescaling thermostat[39] using a 0.1 ps time constant. All water molecules were kept rigid through the RATTLE algorithm,[40] allowing a propagation time step of 1.0 fs. Intermolecular Lennard-Jones interactions were truncated beyond 10 Å. Electrostatic interactions beyond this same cutoff were handled with a PPPM method,[41] with the additional correction proposed by Yeh and Berkowitz for the slab geometry.[42] The total linear momentum of all the systems was removed every 100 fs to prevent collective displacements.

The results on structural, dynamical, and spectroscopic properties of interfacial water molecules were obtained with unbiased simulations in the three geometries described above, with a total simulation time of 2 ns for each system, after equilibrations of 100 ps (bulk systems were equilibrated with a constant pressure of 1 atm). Reference bulk values for all quantities were obtained from a 1 ns-long simulation of 903 water molecules in a 3D-periodic box of side 30.0 Å, previously equilibrated for 100 ps.

The free energy profiles presented for ion solvation and salt dissociation were obtained with umbrella sampling[43] and the required bias potentials were enforced with PLUMED.[44] For ion solvation, an umbrella sampling harmonic bias potential of 10 kcal·mol^{-1}·Å^{-2} was applied either along the distance between the ion and the center of mass of water molecules for the droplet

and cavity systems, or along the vertical distance between the ion and the water center of mass for the slab. A total of 81 window simulations was used for the droplet and cavity systems, and 99 window simulations for the slab system, always evenly spaced by 0.125 Å and with total simulation lengths of 500 ps where the first 100 ps were used as equilibration. We then obtained the free energy profiles along the distance to the average air-water interface of each system by a simple translation of the frame of reference, which ensures that the profiles can be compared between the three systems. Although the distance to the instantaneous interface would be another interesting collective variable, its implementation is far more complex and its computational cost is much larger, while it is not expected to give significantly different surface affinities. For salt dissociation, umbrella sampling harmonic biases of 25 kcal·mol^{-1}·Å^{-2} were applied along the ion-ion distance. We employed 48 windows, evenly spaced by 0.125 Å and of total simulation length of 150 ps where the initial 50 ps were used as equilibration. Free-energy profiles were obtained from these simulations with our own implementation of the weighted histogram analysis method (WHAM),[45] and the errors were computed as prescribed by Zhu and Hummer.[46]

III. RESULTS AND DISCUSSION

The following sections successively present the impact of interfacial curvature on structural properties and their consequences on the vibrational density of states, on dynamical properties, on simple chemical processes including ion solvation and ion pair dissociation.

A. Structural properties: density and molecular orientation

We first define the interfacial water layer whose structural, spectroscopic and dynamical properties will be characterized in the following. We have adopted a geometric definition based on the instantaneous location of the water interface and on the thickness of the interfacial layer. In contrast with the Gibbs dividing surface, which only provides an average location of the interface, we have considered the *instantaneous* interface to follow the interfacial fluctuations and to probe how the interface locally deviates from its average position and shape (plane or sphere), providing a detailed picture of the local solvation environment. Following the procedure in ref. 27, the instantaneous interface is determined as the surface where the instantaneous water density reaches half its bulk value, and its location is computed at every step of the trajectories (see typical examples

in Fig. 1).

The thickness of the interfacial layer is then determined from the molecular density profile along the distance to the instantaneous interface. Figure 2 shows the density profiles for the different systems, together with the density profile in the slab system when the distance to the Gibbs dividing surface is used instead of that to the instantaneous interface. These profiles first show the importance of considering the instantaneous interface to reveal the first layer, since the layered structure is not apparent with the average Gibbs dividing surface.[27,47] Regarding the degree of structuring at interfaces with different curvatures, figure 2 shows that the density of the first layer increases (*i.e.*, the first peak becomes higher and narrower) when going from the droplet to the slab geometry, consistent with the expected increase in surface tension[19] (the first layer density further increases at the cavity interface, but this is at least partly due to the repulsive potential employed in the simulation). For each system we select as the first layer all molecules closer to the interface than the first minimum of these instantaneous density profiles (3 Å for slab and droplet and 2.5 Å for the cavity system). Our identification of interfacial molecules is therefore based on the distance to the instantaneous surface where the density is half its bulk value. But the properties of water are not uniform within this first layer and, as shown by the number of H-bonds in Figure 3, molecules on the liquid side of this interfacial layer are more bulk-like than those on the vapor side. Other methods have been proposed[47,48] whose advantage is to specifically identify the molecules in direct contact with the vapor phase. However, while the definition chosen for the interfacial layer may slightly affect the average values for interfacial properties, it is not expected to impact our conclusions regarding how curvature changes these properties.

We now characterize the orientations of water molecules at the interface. While the bulk liquid is isotropic and the orientation of water molecules is distributed uniformly, the interface with air or with a hydrophobic phase disrupts the H-bond network, which leads to preferential orientations of water molecules, such as the clathrate and anti-clathrate arrangements seen near hydrophobic solutes.[49] Based on simple geometric considerations, one can expect the interfacial curvature to change the number of first shell H-bond partners around an interfacial water molecule and therefore its preferred orientations. For each system, we have therefore computed the distributions of orientations with respect to the instantaneous interfaces for the OH bonds and dipoles of water molecules lying at the interface.

The results are presented in Fig. 4 and we first examine the orientations of OH groups (Fig. 4a). For all three curvatures, interfacial water OH groups exhibit three favored orientations, respec-

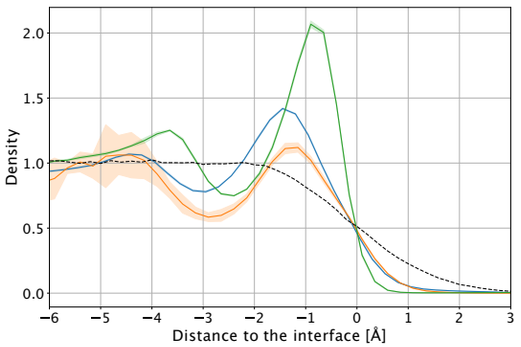

FIG. 2. Molecular density profiles as a function of the distance to the instantaneous air-water interface for the slab (blue), droplet (orange) and cavity (green) systems. Densities are normalized with respect to the densities observed in the "core" of each system, defined as the region farther than 6 Å from the interface. Negative distances indicate the liquid phase. Black dashes show the average water density in the slab geometry.

tively i) dangling towards the vapor or hydrophobic phase ($\cos\theta_{OH} \simeq 1$), ii) approximately tangent to the interface ($\cos\theta_{OH} \simeq 0$) and iii) pointing towards the bulk ($\cos\theta_{OH} \simeq -1$). These three main orientations have already been described in the clathrate and anti-clathrate arrangements of the hydration shell around hydrophobic solutes,[49] including a small dangling fraction,[50] but also at the flat air-water interface,[51] at the water/graphene interface[52–54] and at the water/graphene oxide interface.[55]

A key result revealed by our calculations in Fig. 4 is that the fractions of populations adopting each orientation strongly depend on the interfacial curvature, in agreement with prior studies of the fluctuating negatively and positively curved portions of (on average) flat interfaces.[48] This is particularly striking if we consider the dangling fraction. A quantitative definition of the dangling population and of the maximum angular deviation with respect to the surface normal is necessarily arbitrary. Several geometric criteria have been proposed.[56,57] In this work, we consider that an OH bond is dangling when the angle θ_{OH} formed with the interface normal is such that $\cos\theta_{OH} > 0.75$ (*i.e.* $\theta_{OH} \lesssim 41°$). This condition is based on the location of the minimum in the orientation probability distribution in the droplet, which exhibits the broadest dangling peak distribution. Using this definition, we determine the fraction of interfacial water molecules presenting at least one dangling OH bond in each of the three systems. This dangling fraction is calculated to be respectively

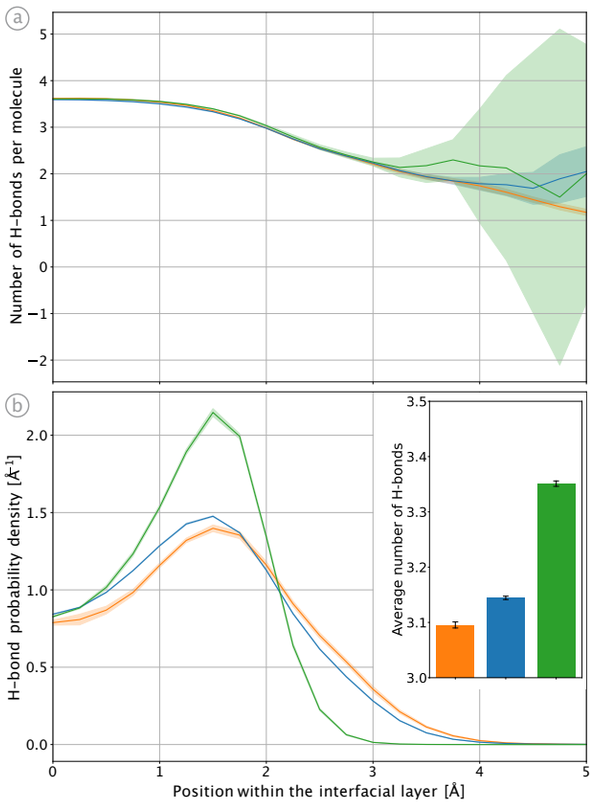

FIG. 3. a) Number of H-bonds for water molecules within the interfacial layer along the distance from the first minimum in the density profile (Figure 2) for the slab (blue), droplet (orange) and cavity (green). Shaded regions show the confidence interval. b) H-bond probability density obtained from the product of the water number density and the number of H-bonds in panel a. The inset provides the average numbers of H-bonds for water molecules within the interfacial layer.

18% in the droplet, 12% in the slab, and 6% in the cavity, showing a pronounced decrease with decreasing curvature, with about three times fewer molecules with a dangling bond in the cavity than in the droplet. Although the exact numbers depend on the geometric definition adopted for the dangling population, the trend between the three systems is expected to be robust. This result is consistent with simple considerations about the geometry of the interface and the proportion of space where water is absent, and in line with previous studies on cavities of growing sizes.[58]

We next consider the orientation of the interfacial water dipoles, shown in Fig. 4b. Our simulations show that while for the three curvatures the dipoles are approximately tangent to the interface, their average orientation points toward the liquid phase, and this asymmetry very slightly increases when the curvature increases from the cavity to the slab and the droplet. The average

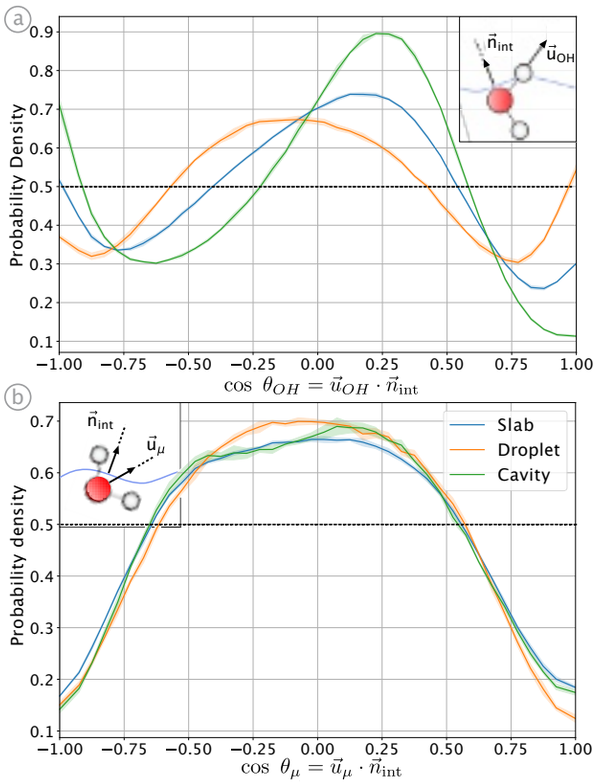

FIG. 4. Orientation probability distributions of the a) OH bond unit vectors $\vec{u}_{OH}$ and b) dipole unit vectors $\vec{u}_{\mu}$ of first layer molecules with respect to the normal to the water interface $\vec{n}_{int}$ oriented towards the vapor phase, for the slab (blue), droplet (orange) and cavity (green) systems. Black dashes indicate the isotropic distribution obtained in bulk conditions.

orientations $\arccos\left(\langle\cos\theta_{\mu}\rangle\right)$ of the interfacial water dipoles obtained from Fig. 4b are 91.0° for the cavity, 91.1° for the slab, and 91.2° for the droplet. This increasing dipole deviation from the surface normal was also observed in previous simulations of growing cavities.[58] This orientation of the interfacial dipoles causes a polarization of the interface, already seen for example at the water/graphene interface.[53] This polarization has very important consequences, since it has for example been suggested[59] to be responsible for the electrophoretic mobility of air bubbles in water[60] that behave as if they were negatively charged despite their zero net charge.

Finally, the curvature-induced change in orientation for the interfacial water molecules also impacts the average number of H-bonds. Figure 3b shows that water molecules are more H-bond coordinated at the interface of the cavity than at the interface of the droplet.

B. Vibrational density of states

We now examine the effects of structural rearrangements within the interfacial layer on the vibrational properties of water, specifically focusing on the water OH bond stretching frequency region. The OH stretch vibration is highly sensitive to the strength of H-bonds, making linear and nonlinear vibrational spectroscopies valuable tools for probing the H-bond structure of water. To selectively characterize the interfacial region, surface-specific nonlinear techniques are particularly attractive. This includes for example vibrational sum-frequency generation that has been extensively used at aqueous interfaces.[61] However, this method requires a flat interface and for curved interfaces, advanced nonlinear scattering techniques have been developed.[25,26,62,63] In the following, we therefore do not focus on a specific type of vibrational spectroscopy and we calculate the vibrational density of states (VDOS) of interfacial water molecules to determine the spectroscopic impact of interfacial curvature.

A number of methods have been used to calculate water vibrational spectra, including, *e.g.*, classical simulations combined with an empirical map,[35,64] charge response kernel-based simulations,[65] ab initio molecular dynamics simulations with velocity autocorrelation function,[66] and neural network-based simulations combined with transition dipole calculations.[67,68] Here we use an empirical map established from semi-classical calculations that relates the OH vibrational frequency to the local electric field experienced by the H atom projected along the OH axis[69] determined from classical molecular dynamics with rigid water molecules. We calculate the vibrational frequency of each water OH stretch mode independently and neglect intra- and intermolecular couplings, which would correspond to the experimental situation of a dilute solution of HOD in D_2O.

The resulting VDOS for interfacial water molecules are presented in Fig. 5. We first examine the distributions normalized over the full 2600–3900 cm^{-1} frequency range (Fig. 5a). All interfacial systems show the same two distinct features: a broad band approximately similar to the bulk density (3000–3600 cm^{-1}) and a high frequency shoulder or peak (above $\approx$ 3700 cm^{-1}). Whereas the broad band arises from water OH groups engaged in H-bonds, the blueshifted frequency peak corresponds to dangling OH groups that are not engaged in H-bonds. Our results show that the amplitude of the dangling OH peak exhibits a pronounced increase with increasing interfacial curvature from the cavity to the slab and to the droplet. This is particularly manifest in the difference between the interfacial and bulk VDOS shown in Fig. 5c. This is consistent with the analysis of the orientational arrangement of interfacial molecules in Fig. 4a which showed an increasing fraction

of dangling OH groups pointing towards the interface when curvature increases.

We then examine whether the interfacial curvature affects the VDOS H-bonded band. We therefore consider the density of states now normalized over the 2600–3500 cm^{-1} interval in order to remove the effect of the changing dangling fraction. Here the 3500 cm^{-1} upper bound for the frequency is chosen to approximately correspond to the peak of the low-frequency distribution but this choice does not affect our conclusions. The resulting VDOS in Fig. 5b and the differences with the bulk density in Fig. 5d show that interfacial curvature has a very small effect on the H-bond strength of the bonded OH groups. For the cavity and slab systems, a moderate depletion in (redshifted) strongly H-bonded groups and a corresponding excess of (blueshifted) weakly H-

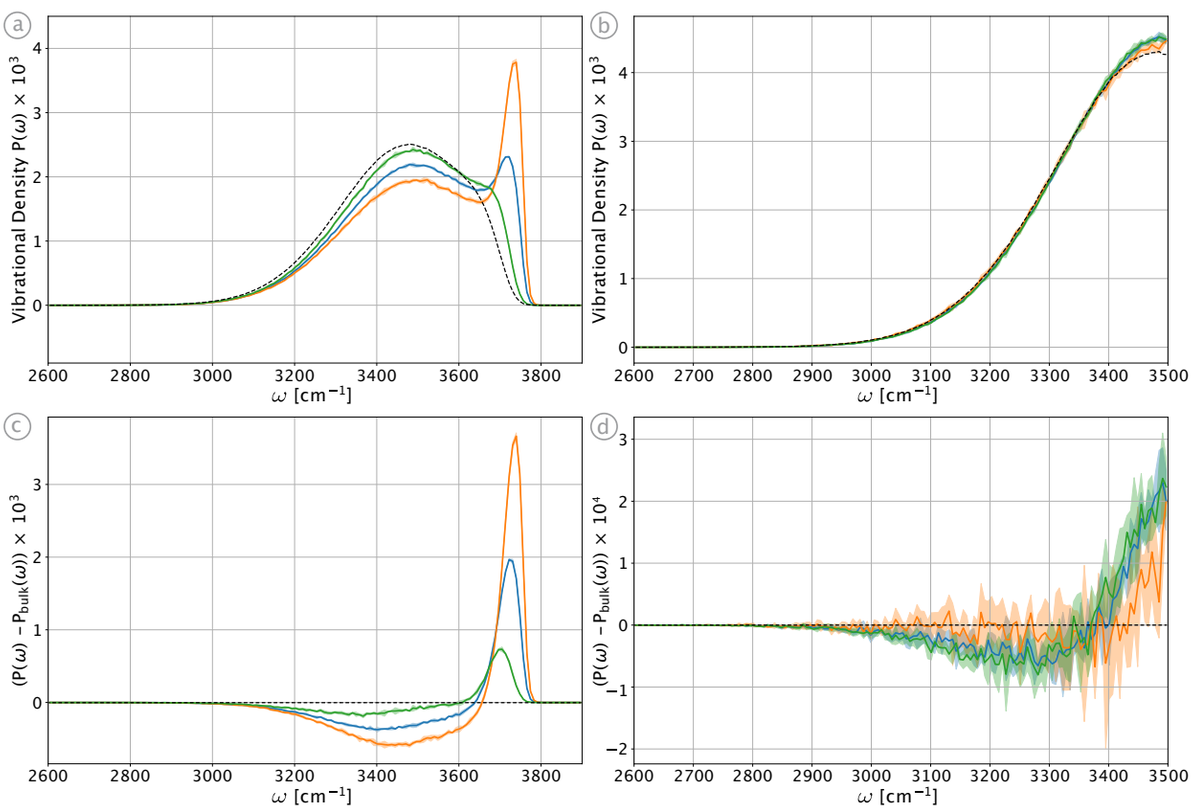

FIG. 5. Vibrational density of states (VDOS) for the OH stretch mode of interfacial water molecules in the slab (blue), in the droplet (orange), in the cavity (green), together with the bulk reference (black dashes). a) VDOS normalized over the 2600–3900 cm^{-1} OH water stretch frequency domain. b) VDOS normalized over an arbitrarily chosen low-frequency 2600–3500 cm^{-1} H-bonded region. c) Difference between the interfacial and bulk VDOS shown in a). d) Difference between the interfacial and bulk VDOS shown in b. 95% confidence intervals are represented by shaded areas.

bonded groups are observed, while this effects appears to be even more limited in the droplet. However, we note that the amplitudes of these changes are close to our uncertainty intervals.

A molecular interpretation of the changes in the VDOS for the H-bonded OH groups is provided by the analysis of the geometric distortions for the interfacial H-bonds. Figure 6 focuses on H-bonded interfacial OH groups (see the geometric H-bond definition in Figure 6a) and considers the probability distribution along the d_{OO} donor-acceptor distance and along the ϕ HOO angle. First, we examine the effect of a flat interface on the H-bond geometry compared to bulk and Figure 6b shows that interfacial H-bonds tend to be longer and more angularly distorted. This is consistent with the depletion in redshifted OH groups and enrichment in blueshifted OH groups in the VDOS in Figure 5d. However, the curvature effect on the interfacial H-bond geometry is very limited, as shown by Figure 6c-d, and consistent with the similar VDOS for all three curvatures in Figure 5d.

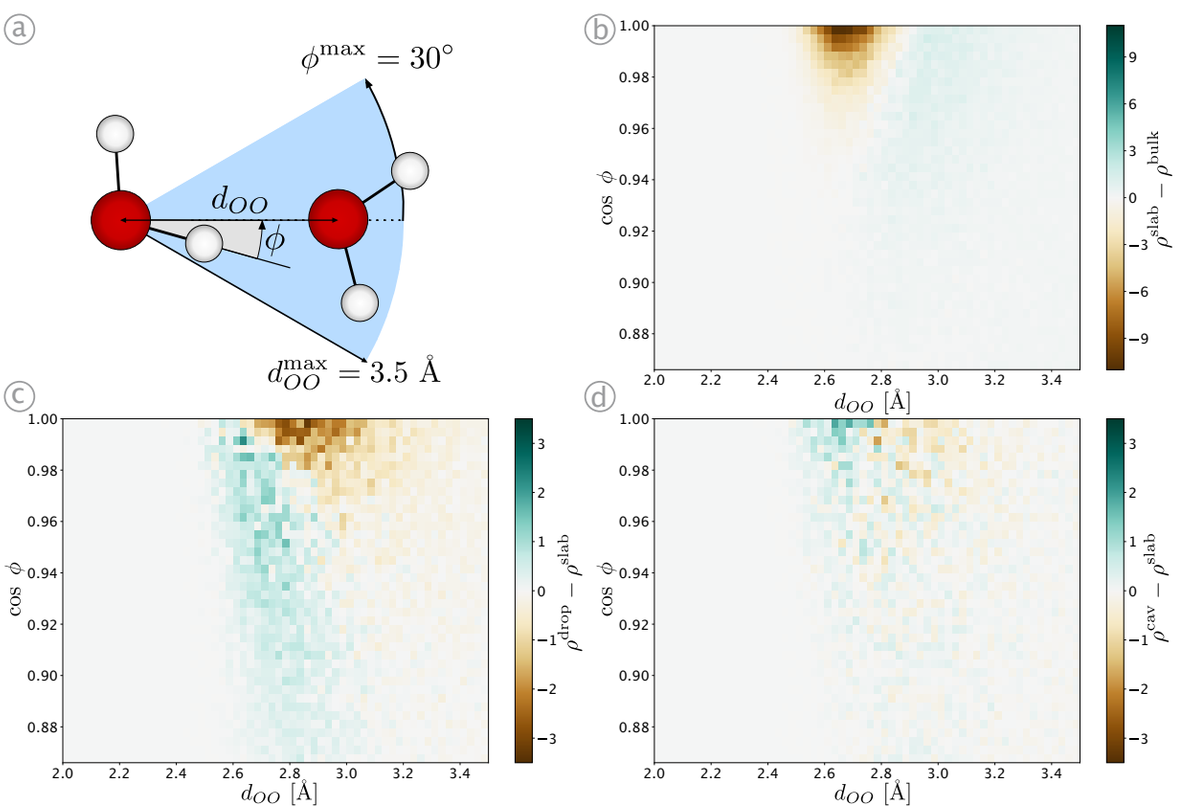

FIG. 6. a) Geometric definition of H-bonded water OH groups. b) Probability density difference of H-bonded OH groups along the d_{OO} donor-acceptor distance and along the ϕ HOO angle between the slab interface and bulk water. c) Probability density difference between the droplet interface and the slab interface. d) Probability density difference between the cavity interface and the slab interface.

Our simulations over a broad range of curvatures therefore show that while curvature strongly impacts the fraction of H-bonded interfacial water OH groups, it does not induce a substantial change in the strength of the H-bonds that are formed. While we cannot exclude that these effects could be more pronounced with calculations including, *e.g.*, polarization, we do not expect the impact of curvature alone to explain the large ≈ 200 cm^{-1} frequency redshift observed in the experimental spectra of water at μm-sized curved interfaces with oil,[25,26] which suggests that other contributions should be considered. It was for example recently proposed[70] that H-bond-mediated charge transfer between water and oil could explain the anomalous spectroscopic signature of the water-oil droplet interface. However, why charge transfer would be different at curved droplet interfaces and at planar interfaces remains unexplained.

C. Dynamical properties: diffusion, reorientation and H-bond jumps

We now turn to the determination of the curvature's impact on the dynamical properties of water. In the bulk, H-bond exchanges have been established to be the key determinant of water translational[71] and reorientational[72] dynamics. Previous studies on a series of flat interfaces with different polarities have shown[53,56,73,74] how the orientation of interfacial water molecules impacts the interfacial dynamics. Here we extend these studies to determine the effect of curvature.

We first consider the translational dynamics of interfacial water molecules. In contrast to the isotropic bulk situation, the air-water interface exhibits a broken local symmetry so that diffusion is not equivalent in the directions parallel and orthogonal to the interface. In addition, along the axis perpendicular to the interface, water molecules diffuse on a potential of mean force which is not flat. Determining the diffusion tensor from simulations is therefore not as straightforward as in the bulk.[75] In order to provide a simple comparison between our systems and prior work,[76] we computed the (three-dimensional) mean squared displacement (MSD) of water molecules initially lying within the interfacial layer, and we determined the average time Δt for a water molecule to diffuse over a distance equal to the thickness of the interfacial layer, approximated to be 3 Å here.

The MSDs for the three systems are presented in Fig. 7. Their slope increases with increasing curvature from the cavity to the slab and to the droplet: the slope at the droplet interface is approximately 1.5 times larger than at the slab interface, and approximately 2.5 times larger than at the cavity interface. Consequently, the characteristic diffusion time Δt decreases with increasing curvature, as shown by the values reported in Table I. The accelerated dynamics of interfacial water

molecules in slab systems have already been determined in previous works.[75,77] The acceleration factors with respect to bulk water depend on the water model and on the interface definition, but are consistent with the ≈ 1.5 factor found here (see Table I).

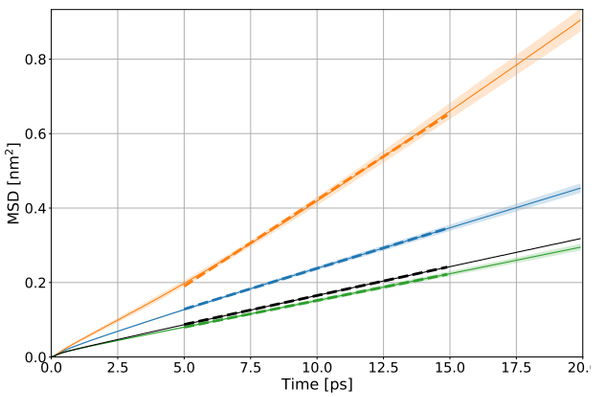

FIG. 7. Mean squared displacements of water molecules initially within the interfacial layer of the cavity (green), of the slab (blue) and of the droplet (orange), together with the bulk reference (black). Dashed lines show the results of linear fittings and shaded areas indicate 95% confidence intervals.

	Translation	Reorientation	H-bond
	Δt [ps]	$\langle \tau^{\text{reor}} \rangle$ [ps]	$\tau_j^{B\to(B,D)}$ [ps]
Cavity	5.7	2.95	3.8
Slab	3.4	2.33	3.6
Droplet	2.3	1.69	3.4
Bulk	5.3	2.53	3.24

TABLE I. Characterization of the dynamics of water molecules initially within the interfacial layer for systems with different curvatures. Average diffusion time Δt over 3 Å, average water OH reorientation times $\langle \tau^{\text{reor}} \rangle$ from eq. 3, and H-bond jump time $\tau_j^{B\to(B,D)}$. 95% confidence errors are approximately 0.2 ps.

As we show now, interfacial reorientation dynamics exhibits the same acceleration with increasing curvature as the translational dynamics. We characterize the reorientation of interfacial water molecules via the reorientation time-correlation function

$$C_{\text{reor}}(t) = \langle P_2 \left[\mathbf{u}_{OH}(0) \cdot \mathbf{u}_{OH}(t) \right] \rangle \tag{1}$$

where P_2 is the second rank Legendre polynomial, $\mathbf{u}_{OH}$ is the unit vector along the water OH bond direction (see inset Fig. 4) and the average is performed over all water molecules initially lying within the interfacial layer. In the bulk, $C_{\text{reor}}(t)$ is accessible experimentally via time-resolved infrared spectroscopy.[78–80]

The time-correlation functions calculated from our simulations are shown in Fig. 8. They exhibit the same trend as the translational dynamics in Fig. 7, with increasingly fast reorientation dynamics when the curvature increases from the cavity to the slab and to the droplet.

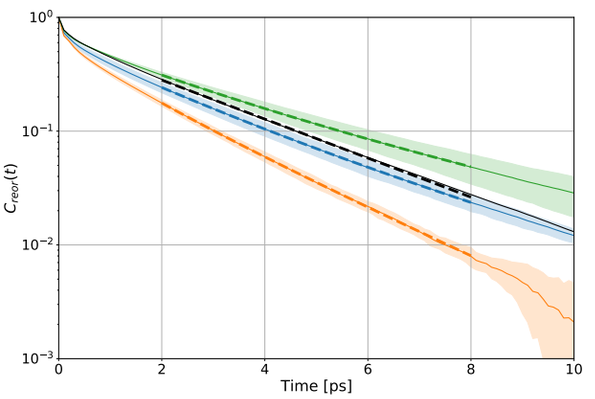

FIG. 8. Reorientation time correlation function eq. 1 for the OH bonds of water molecules initially lying within the interfacial layer (solid lines) for the slab (blue), droplet (orange) and cavity (green), together with the bulk (black). Dashed lines show the bi-exponential fit eq. 2 over the 2–8 ps range and shaded regions represent the 95% confidence intervals.

In the bulk, the simulated time-correlation function beyond the librational timescale is well approximated by a single exponential decay with a characteristic timescale of 2.5 ps, in excellent agreement with experiments and with previous simulations.[78–81] At interfaces however, this long-time decay becomes multiexponential. Previous studies at flat interfaces showed that this arises from the different H-bonded populations with distinct reorientation times.[53,56,73,74] To characterize this decay, we therefore describe it with the bi-exponential form

$$C_{\text{reor}}(t) = ae^{-t/\tau_a^{\text{reor}}} + be^{-t/\tau_b^{\text{reor}}} \tag{2}$$

and define the average reorientation time as the weighted average of the two relaxation times

$$\langle \tau_{\text{reor}} \rangle = \frac{a}{a+b}\tau_a^{\text{reor}} + \frac{b}{a+b}\tau_b^{\text{reor}} \tag{3}$$

The average reorientation times obtained from the parameters of eq. 2 adjusted over the 2–8 ps interval are given in Table I. They show that water reorientational dynamics at the interface of the cavity, slab and droplet systems exhibits the same trend as translational dynamics: water dynamics is faster when the curvature increases: $\langle \tau_{\text{reor}} \rangle$ is 1.7 times faster in the droplet than in the cavity, and 1.3 times faster in the droplet than in the slab.

Previous studies have established that bulk translational and reorientational dynamics are governed by H-bond exchange dynamics.[71,72] Stable exchanges of H-bond partners induce both a large amplitude OH reorientation and a translational displacement of the water oxygen atom. Jump models were shown to successfully relate these H-bond exchanges to the translational[71] and reorientational[72] dynamics. Further extensions of the jump model at flat interfaces[53,56,73,74] and at biomolecular interfaces[82,83] determined that the average water reorientation time results from the different populations of water OH groups, with distinct orientations and distinct H-bond exchange dynamics. In the following we now analyze the effect of curvature on H-bond dynamics to understand the interfacial translational and reorientational dynamics described above.

The H-bond exchange of an H-bond donating water OH group between its initial and final H-bond accepting partners is described as a chemical reaction. Jump times are determined from the cross time correlation function between the initial (I) and final (F) states

$$C_j(t) = 1 - \langle p_I(0) p_F(t) \rangle \tag{4}$$

where $p_{I,F}(t)$ is 1 if the system is in state I (resp. F) and 0 otherwise. States I and F are defined within the Stable States Picture[81] using strict geometric criteria to remove contributions from rapid, unproductive, barrier crossing events, and absorbing boundary conditions in the product state ensure that the forward rate constant is calculated. We determine the jump time for water OH groups at the interface to go from an initial stable H-bonded acceptor (state B defined by the geometric conditions OO$<$3.1 Å and $\hat{HOO} <15^\circ$), to a final state where the OH group is either H-bonded to a different stable acceptor (state B) or in a stable dangling state (state D, defined by an angle between the OH bond and the surface normal below 30°).

The jump time-correlation functions are presented in Fig. 9 and the jump times obtained by exponential fitting are reported in Table I. They show that the jump dynamics of interfacial and initially H-bonded water OH groups are quite similar in the three systems with different curvatures. The $\tau_j^{B\to(B,D)}$ jump time decreases by less than 10% between the slowest cavity system and the fastest droplet system. This can be understood by considering the two key factors which have been

shown to determine the H-bond jump time.

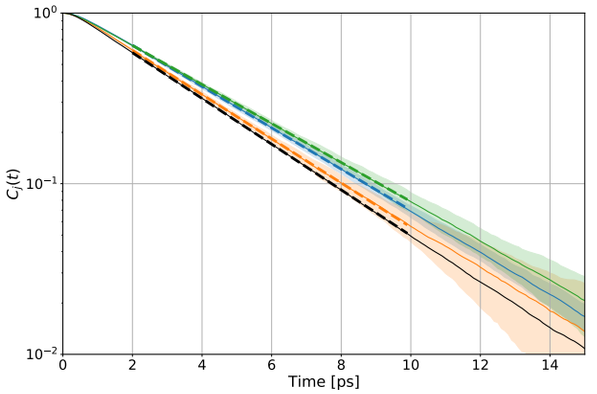

FIG. 9. H-bond jump time-correlation function eq. 4 of water OH groups initially lying in the first interfacial layer of the slab (blue), the droplet (orange) and the cavity (green), together with the bulk reference (black). Dashed lines show the exponential fitting on the 2–10 ps interval, with the resulting jump times in Table I and colored shaded regions represent the 95% confidence intervals.

The first one is the entropic excluded-volume factor, which slows down H-bond jumps occuring at an interface where part of the surrounding space is devoid of potential new H-bond acceptors.[82,84] Previous studies[53,73,74] showed that near an apolar interface, the excluded volume factor slows down the time to jump from an initial stable acceptor to another stable acceptor. However, here we consider the time to jump from an initial acceptor (state B) to either another stable acceptor (state B) or to a dangling situation (state D), and the excluded volume factor therefore does not affect this global jump time.

The second factor affecting the jump time is the strength of the initial H-bond that needs to be elongated to reach the jump transition state:[82] stronger initial H-bonds cause a slowdown of the jump dynamics. The determination of the VDOS (Fig. 5) indicated that H-bonded OH groups have similar strengths in all three systems, and the jump H-bond strength effect is expected to be negligible.

Consideration of the excluded volume and H-bond strength factors thus explains that the $\tau_j^{B\to(B,D)}$ jump time changes very little with curvature. The acceleration of interfacial water translational and reorientational dynamics with increasing curvature therefore does not result from a change in the dynamics of H-bonded water OH groups. However, the structural and spectroscopic characterization of the interface in Figs. 3, 4 and 5 showed that the fraction of H-bonded OH groups at the interface decreases markedly with increasing curvature, due to the growing fraction

of dangling OH groups. This has important consequences for water translational and rotational dynamics. First, the reduced average coordination of water molecules implies that H-bond jump events induce larger translational displacements[71] of water molecules compared to the bulk, which leads to the acceleration of interfacial dynamics, well-known for the case of flat surfaces.[75,77] Second, dangling OH groups exhibit fast and large-amplitude reorientational dynamics since they are not H-bonded and there is no cost to reach the jump transition state.[53,56,73,74] This implies that the decreasing H-bond coordination and growing fraction of fast dangling OH groups with increasing curvature accelerate the translational and reorientational dynamics of interfacial molecules.

D. Solvation: halide hydration free energies

We now examine whether the changes in structure and dynamics caused by interfacial curvature affect simple chemical phenomena, and we first consider the solvation of ions. In the following, we will determine how the hydration free energies of fluoride and iodide anions change with the distance to the interface for the cavity, slab and droplet systems.

The hydration free energy profiles of the two ions along the distance to the interface are presented in Fig. 10. Although our simulations employ a non-polarizable force field, they correctly describe the well known[85] qualitative difference between the surface affinities of the two halide ions. While the fluoride anion is strongly hydrophilic and destabilized when partly desolvated at the interface (Fig. 10a), the iodide anion is surface active and its free energy profile exhibits a minimum at the interface (Fig. 10b).

We now examine the impact of curvature on these solvation free energy profiles. While the slab and droplet systems can be compared directly since they both have a free water surface, the cavity simulation employed a Lennard-Jones potential to mimic an apolar oily phase. The latter affects the ion free energy profile, causing for example its strong increase when the ion moves into the apolar phase, and its dispersive part is also expected to bring an interfacial stabilization, which makes the comparison with other curvatures less straightforward.

We therefore focus on the change in curvature between the droplet and the slab. We first consider the non-surface-active fluoride anion (Fig. 10a). It shows identical hydration free energy profiles in the droplet and slab systems, despite the very pronounced change in curvature. Furthermore, approximately 4 Å below the instantaneous interface, the three systems show hydration free energies that are identically converged to the free energy value in the core of the systems.

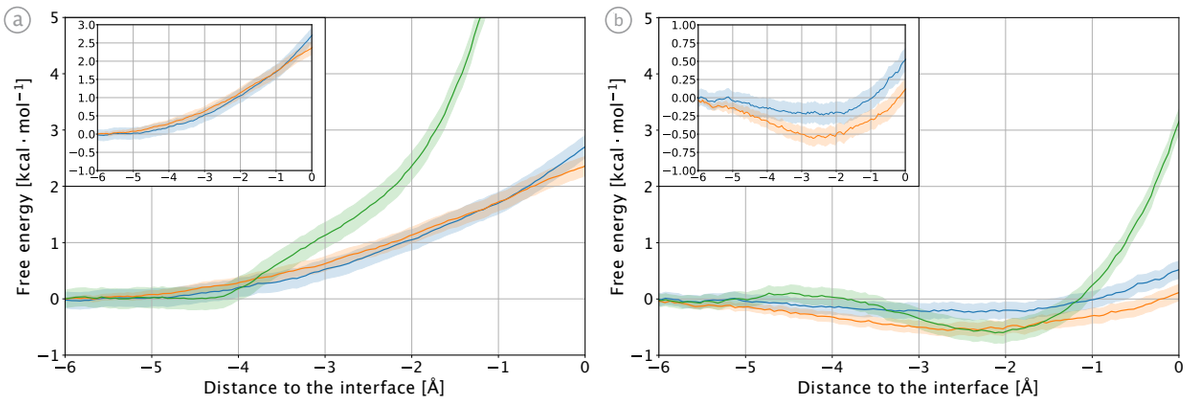

FIG. 10. Hydration free energy profiles in the slab (blue), droplet (orange) and cavity (green) systems a) for a fluoride anion and b) for an iodide anion. For the cavity and droplet spherical systems, the profiles have been corrected for the change in accessible volume along the distance to the interface. Shaded regions represent the 95% confidence interval and negative distances indicate the condensed water phase. Inset panels compare the slab (blue) and droplet (orange) profiles, with the same axes labels as for the main figures.

We then turn to the larger and slightly surface active iodide anion (Fig. 10b). Its stabilization at the interface compared to the core of the systems is -0.2 kcal·mol^{-1} in the slab and -0.5 kcal·mol^{-1} in the droplet, which suggests that the ion is increasingly stabilized when the interfacial curvature increases. Although this change in interfacial hydration free energy for the iodide anion is outside our uncertainty intervals (0.2 kcal·mol^{-1}), it remains well below the thermal energy at 300 K, suggesting that changes in the solvation properties of the droplet interface are very moderate. In addition, the classical forcefields used here were not specifically parameterized for ion solvation and do not account for ion polarizability, and such a small free energy difference should not be over interpreted.

What is clearly shown by our simulated free energy profiles is that curvature does not change the hydration free energy of ions by much more than the thermal energy. Consequently, curvature effects probably cannot explain the anomalous reactivity changes observed at soft water interfaces.

E. Simple chemical process: ion pair dissociation

Finally, we consider a simple reactive process, the dissociation of a sodium fluoride ion pair. For this study, instead of the droplet, slab and cavity systems used so far, we focus on two nan-

odroplets of 256 and 512 water molecules, which present different curvature radii of 11.6 Å and 14.9 Å respectively. With respect to the previous analyses, the objective is to assess whether a finite change in the curvature radius of a nano system has an overall impact on reactivity, without restraining the analysis to the outmost layer. Therefore in our simulations, only the distance between the two ions is controlled, but the ions are free to diffuse within the droplets.

The dissociation free energy profiles along the ion-ion distance in the two droplets (Fig. 11) present the three local free energy minima typical of ion pairing processes, corresponding respectively to the contact ion pair (CIP), solvent-shared ion pair (SIP) and solvent separated ion pair (SSIP) structures.[86] The first local minimum, at an ion-ion distance of $r_{\text{ion}} \simeq 2.4$ Å, corresponds to the contact ion pair. At distances between 4 Å and 5 Å, the free energy profiles exhibit a broad local minimum, which corresponds to the solvent-shared pair state. Finally, after a small barrier, the profiles flatten again, which corresponds to the solvent-separated ion pair state. We report the free energy differences between the contact ion pair and the solvent-shared and solvent-separated states in Table II, which are in good agreement with experimental measurements of sodium fluoride dissociation ratios.[87]

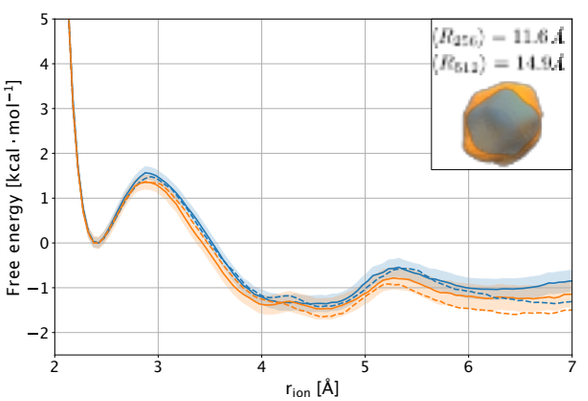

FIG. 11. Free energy profiles along the inter-ionic distance r_{ion} of a sodium fluoride ion pair within 256-water (solid blue line) and 512-water (solid orange line) droplets and in bulk solutions with the same concentration (dashes). The inset depicts typical shapes of the instantaneous water interfaces of both systems along with their average radii. At this nanometric scale, the instantaneous configurations of both systems strongly deviate from the average spherical geometries. 95% confidence intervals for the droplet profiles are represented as shaded regions; the bulk confidence intervals are approximately identical and not shown for clarity reasons.

We now examine the impact of droplet curvature on the ion pair dissociation thermodynamics.

Number of water molecules	256	512
$\Delta_r G_{\mathrm{CIP}\rightarrow\mathrm{SIP}}$ [kcal·mol^{-1}]	-1.3 (-1.4)	-1.5 (-1.6)
$\Delta_r G_{\mathrm{CIP}\rightarrow\mathrm{SSIP}}$ [kcal·mol^{-1}]	-1.0 (-1.3)	-1.2 (-1.6)

TABLE II. Dissociation free energy from the contact ion pair (CIP) to the solvent-shared ion pair (SIP) $\Delta_r G_{\mathrm{CIP}\rightarrow\mathrm{SIP}}$ and from the CIP to the solvent-separated ion pair (SSIP) $\Delta_r G_{\mathrm{CIP}\rightarrow\mathrm{SSIP}}$ in the droplets with 256 and 512 water molecules. Values in bulk solutions with the same concentration are given between parentheses. The half widths of the 95% confidence intervals are 0.1 kcal·mol^{-1} for $\Delta_r G_{\mathrm{CIP}\rightarrow\mathrm{SIP}}$ and 0.2 kcal·mol^{-1} for $\Delta_r G_{\mathrm{CIP}\rightarrow\mathrm{SSIP}}$.

Figure 11 shows that dissociation free energy profiles in the two systems have the same shape, with a very moderate destabilization of the dissociated SSIP state by approximately 0.2 kcal·mol^{-1} between the larger droplet and the smaller droplet.

However, the smaller and larger droplet systems differ not only by their curvature, but also by their ion concentration. We therefore performed two reference bulk situations with the same concentrations as in the droplets (see Methods). The computed bulk free energy profiles are shown as dashed lines in Fig. 11. The same change as between the smaller and larger droplet free energy profiles is found between the lower and higher concentration bulk solutions. This suggests that this change is caused by the ion concentration and not by the droplet curvature.

The only noticeable change between the droplet and bulk systems with same concentration is the relative destabilization of the SSIP state in the droplet system by approximately 0.3 kcal·mol^{-1} with respect to the bulk value. This increase is identical for both system sizes and is probably due to the fact that, since neither fluoride anions nor sodium cations are surface active, constraints at larger ion-ion separations in these finite-sized droplets force the ions to be partially desolvated. (In the case of ion dissociation at a flat air-water interface, the impact of the interface has already been determined[88]). Our simulations therefore show that despite a 20% curvature increase between the larger and smaller droplets, ion dissociation free energies in the core regions of such systems are not significantly affected.

In addition to their curved interface, droplets have a number of properties that distinguish them from bulk solutions and that could have impacted the ion dissociation process. These include for example their permittivity. It has been shown both experimentally[89] and via simulations[90–93] that at the interface between water and a low dielectric medium, the permittivity of the interfacial water

layer along the direction perpendicular to the interface is significantly reduced with respect to the bulk. This could have been expected to lead to a reduced solvation of the dissociated ion pair and to increase the pair dissociation free energy. However, the interfacial permittivity along the direction parallel to the interface has been shown to be enhanced compared to the bulk.[90–93] Our simulations suggest that although this may have an impact when both ions are at the interface,[88] within the droplet the net effect of the changes in the perpendicular and parallel components of the local permittivity on the ion pair dissociation process remains limited.

Another distinguishing feature of small droplets is the Laplace pressure caused by their curvature. In the following we ignore the well-known[19] decrease in surface tension with decreasing droplet size in order to provide an approximate upper bound for the impact of pressure effects. The pressure difference between the exterior and interior of the droplet is $\Delta P = 2\gamma/R$ where $\gamma \simeq 72$ mN/m is the water surface tension and R is the droplet radius. Between the two droplets in our simulations with R_1=11.6 Å and R_2=14.9 Å, the change in Laplace pressure is $\Delta\Delta P = 2\gamma(1/R_1 - 1/R_2) \simeq 275$ bar. The change in molar volume upon dissociation of the NaF ion pair has been estimated in the literature[94] to be ΔV=-4.77 cm^3/mol at infinite dilution. The impact of the different curvatures and of the substantial change in Laplace pressures on the ion pair dissociation free energy is therefore limited to $\Delta\Delta P \times \Delta V \simeq 0.03$ kcal/mol. In contrast, when a single ion pair is dissociated in droplets of different sizes, the effect of concentration on the dissociation free energy can be estimated for an ideal solution to be $k_B T \ln(V_1/V_2) = 3k_B T \ln(R_1/R_2) \simeq 0.4$ kcal/mol, which is clearly dominant over the curvature-induced Laplace pressure term.

IV. CONCLUSION

Using classical molecular dynamics simulations, we have obtained a detailed characterization of the impact of interfacial curvature on a series of key structural, spectroscopic, dynamic and thermodynamic properties of water molecules. Our results show that while increasing the interfacial curvature from a cavity to a slab and to a droplet does not significantly change the strength of H-bonds at the water surface, it strongly increases the proportion of free dangling OH groups. The reduced H-bond coordination at the interface leads to the acceleration of water translational and reorientational dynamics, while the dynamics of H-bond exchanges for H-bonded interfacial molecules is little affected by curvature. Regarding simple chemical processes, our simulations show that curvature has a very limited impact both on ion hydration free energies and on ion pair

dissociation free energies, even for highly curved nanometric systems relevant for fields ranging from atmospheric chemistry to "on-droplet" catalysis. This suggests that interfacial curvature is not likely to play a major role in the distinct chemical reactivity observed at soft water interfaces compared to that in bulk solutions.

ACKNOWLEDGMENTS

This work has been supported through a CDSN Ph.D. fellowship to M. P. from the French Ministry of Higher Education and by an HPC allocation from GENCI-IDRIS (2023-A0130707156).

DATA AVAILABILITY STATEMENT

The data that support the findings of this study are available from the corresponding author upon reasonable request.

REFERENCES

[1]S. Cerveny, F. Mallamace, J. Swenson, M. Vogel, and L. Xu, "Confined water as model of supercooled water," Chem. Rev. **116**, 7608–7625 (2016).

[2]S. M. A. Malek, P. H. Poole, and I. Saika-Voivod, "Thermodynamic and structural anomalies of water nanodroplets," Nat. Commun. **9**, 1–9 (2018).

[3]M. F. Ruiz-Lopez, J. S. Francisco, M. T. Martins-Costa, and J. M. Anglada, "Molecular reactions at aqueous interfaces," Nat. Rev. Chem. **4**, 459–475 (2020).

[4]Z. Wei, Y. Li, R. G. Cooks, and X. Yan, "Accelerated reaction kinetics in microdroplets: Overview and recent developments," Annu. Rev. Phys. Chem. **71**, 31–51 (2020).

[5]N. Aluru, F. Aydin, M. Bazant, D. Blankschtein, A. Brozena, J. de Souza, M. Elimelech, S. Faucher, J. Fourkas, V. Koman, M. Kuehne, H. Kulik, H. Li, Y. Li, Z. Li, A. Majumdar, J. Martis, R. Misra, A. Noy, T. Pham, H. Qu, A. Rayabharam, M. Reed, C. Ritt, E. Schwegler, Z. Siwy, M. Strano, Y. Wang, Y. Yao, C. Zhan, and Z. Zhang, "Fluids and electrolytes under confinement in single-digit nanopores." Chem. Rev. **123**, 2737–2831 (2023).

[6]S. Narayan, J. Muldoon, M. G. Finn, V. V. Fokin, H. C. Kolb, and K. B. Sharpless, ""On Water": Unique Reactivity of Organic Compounds in Aqueous Suspension," Angew. Chem. Int. Ed. **44**, 3275–3279 (2005).

[7]R. M. Bain, S. Sathyamoorthi, and R. N. Zare, ""on-droplet" chemistry: The cycloaddition of diethyl azodicarboxylate and quadricyclane," Angew. Chem. Int. Ed. **56**, 15083–15087 (2017).

[8]S. Enami, Y. Sakamoto, and A. J. Colussi, "Fenton chemistry at aqueous interfaces," Proc. Natl. Acad. Sci. U.S.A. **111**, 623–628 (2014).

[9]L. Qiu, Z. Wei, H. Nie, and R. G. Cooks, "Reaction Acceleration Promoted by Partial Solvation at the Gas/Solution Interface," ChemPlusChem **86**, 1362–1365 (2021).

[10]M. de la Puente, R. David, A. Gomez, and D. Laage, "Acids at the edge: Why nitric and formic acid dissociations at air-water interfaces depend on depth and on interface specific area." J. Am. Chem. Soc. **144**, 10524–10529 (2022).

[11]M. de la Puente and D. Laage, "How the acidity of water droplets and films is controlled by the air-water interface," J. Am. Chem. Soc. **145**, 25186–25194 (2023).

[12]D. Ben-Amotz, "Interfacial chemical reactivity enhancement." J. Chem. Phys. **160**, 084704 (2024).

[13]M. F. Ruiz-López and M. T. C. Martins-Costa, "Disentangling reaction rate acceleration in microdroplets," Phys. Chem. Chem. Phys. **24**, 29700–29704 (2022).

[14]J. K. Lee, H. S. Han, S. Chaikasetsin, D. P. Marron, R. M. Waymouth, F. B. Prinz, and R. N. Zare, "Condensing water vapor to droplets generates hydrogen peroxide," Proc. Natl. Acad. Sci. U.S.A. **117**, 30934–30941 (2020).

[15]H. Xiong, J. Lee, R. Zare, and W. Min, "Strong electric field observed at the interface of aqueous microdroplets." J. Phys. Chem. Lett. **11**, 7423–7428 (2020).

[16]H. Hao, I. Leven, and T. Head-Gordon, "Can electric fields drive chemistry for an aqueous microdroplet?" Nat. Commun. **13**, 280 (2022).

[17]M. Riva, J. Sun, V. F. McNeill, C. Ragon, S. Perrier, Y. Rudich, S. A. Nizkorodov, J. Chen, F. Caupin, T. Hoffmann, and C. George, "High Pressure Inside Nanometer-Sized Particles Influences the Rate and Products of Chemical Reactions," Environ. Sci. Technol. **55**, 7786–7793 (2021).

[18]S. S. Petters, "Constraints on the Role of Laplace Pressure in Multiphase Reactions and Viscosity of Organic Aerosols," Geophys. Res. Lett. **49**, e2022GL098959 (2022).

[19]R. C. Tolman, "The effect of droplet size on surface tension," J. Chem. Phys. **17**, 333–337 (1949).

[20]A. Sanfeld, K. Sefiane, D. Benielli, and A. Steinchen, "Does capillarity influence chemical reaction in drops and bubbles? A thermodynamic approach," Adv. Colloid Interface Sci. **86**, 153–193 (2000).

[21]A. Sanfeld and A. Steinchen, "Does the size of small objects influence chemical reactivity in living systems?" C.R. Biol. **326**, 141–147 (2003).

[22]K. Lum, D. Chandler, and J. D. Weeks, "Hydrophobicity at small and large length scales," J. Phys. Chem. B **103**, 4570–4577 (1999).

[23]S. Rajamani, T. M. Truskett, and S. Garde, "Hydrophobic hydration from small to large length-scales: Understanding and manipulating the crossover," Proc. Natl. Acad. Sci. U. S. A. **102**, 9475–9480 (2005).

[24]I. V. Stiopkin, C. Weeraman, P. A. Pieniazek, F. Y. Shalhout, J. L. Skinner, and A. V. Benderskii, "Hydrogen bonding at the water surface revealed by isotopic dilution spectroscopy," Nature **474**, 192–195 (2011).

[25]S. Pullanchery, S. Kulik, and S. Roke, "Water Structure at the Hydrophobic Nanodroplet Surface Revealed by Vibrational Sum Frequency Scattering Using Isotopic Dilution," J. Phys. Chem. B **126**, 3186–3192 (2022).

[26]N. Smolentsev, W. J. Smit, H. J. Bakker, and S. Roke, "The interfacial structure of water droplets in a hydrophobic liquid," Nat. Commun. **8**, 15548 (2017).

[27]A. P. Willard and D. Chandler, "Instantaneous Liquid Interfaces," J. Phys. Chem. B **114**, 1954–1958 (2010).

[28]G. Ruocco, M. Sampoli, A. Torcini, and R. Vallauri, "Molecular dynamics results for stretched water," J Chem Phys **99**, 8095–8104 (1993).

[29]H. E. Stanley, M. Barbosa, S. Mossa, P. Netz, F. Sciortino, F. W. Starr, and M. Yamada, "Statistical physics and liquid water at negative pressures," Physica A Stat Mech Appl **315**, 281–289 (2002).

[30]H. J. C. Berendsen, J. R. Grigera, and T. P. Straatsma, "The missing term in effective pair potentials," J. Phys. Chem. **91**, 6269–6271 (1987).

[31]C. Vega and E. de Miguel, "Surface tension of the most popular models of water by using the test-area simulation method," J. Chem. Phys. **126**, 154707 (2007).

[32]B. M. Auer and J. L. Skinner, "Vibrational Sum-Frequency Spectroscopy of the Water Liquid/Vapor Interface," J. Phys. Chem. B **113**, 4125–4130 (2009).

[33]Y. Ni and J. Skinner, "Communication: Vibrational sum-frequency spectrum of the air-water interface, revisited." J. Chem. Phys. **145**, 031103 (2016).

[34]J. Schmidt, S. Roberts, J. Loparo, A. Tokmakoff, M. Fayer, and J. Skinner, "Are water simulation models consistent with steady-state and ultrafast vibrational spectroscopy experiments?"

Chem. Phys. **341**, 143–157 (2007).

[35]J. R. Schmidt, S. A. Corcelli, and J. L. Skinner, "Pronounced non-Condon effects in the ultrafast infrared spectroscopy of water," J. Chem. Phys. **123**, 044513 (2005).

[36]I. S. Joung and T. E. Cheatham, "Determination of Alkali and Halide Monovalent Ion Parameters for Use in Explicitly Solvated Biomolecular Simulations," J. Phys. Chem. B **112**, 9020–9041 (2008).

[37]S. Plimpton, "Fast Parallel Algorithms for Short-Range Molecular Dynamics," J. Comput. Phys. **117**, 1–19 (1995).

[38]A. P. Thompson, H. M. Aktulga, R. Berger, D. S. Bolintineanu, W. M. Brown, P. S. Crozier, P. J. in 't Veld, A. Kohlmeyer, S. G. Moore, T. D. Nguyen, R. Shan, M. J. Stevens, J. Tranchida, C. Trott, and S. J. Plimpton, "LAMMPS - a flexible simulation tool for particle-based materials modeling at the atomic, meso, and continuum scales," Comput. Phys. Commun. **271**, 108171 (2022).

[39]G. Bussi, D. Donadio, and M. Parrinello, "Canonical sampling through velocity rescaling," J. Chem. Phys. **126**, 014101 (2007).

[40]H. C. Andersen, "Rattle: A "velocity" version of the shake algorithm for molecular dynamics calculations," J. Comput. Phys. **52**, 24–34 (1983).

[41]R. Hockney and J. Eastwood, *Computer Simulation Using Particles (1st ed.)* (CRC Press., Boca Raton, FL, 1988).

[42]I.-C. Yeh and M. L. Berkowitz, "Ewald summation for systems with slab geometry," J. Chem. Phys. **111**, 3155–3162 (1999).

[43]G. M. Torrie and J. P. Valleau, "Monte Carlo Free Energy Estimates Using Non-Boltzmann Sampling: Apllication To The Sub-Critical Lennard-Jones Fluid," Chem. Phys. Lett. **28**, 578–581 (1974).

[44]G. A. Tribello, M. Bonomi, D. Branduardi, C. Camilloni, and G. Bussi, "PLUMED 2: New feathers for an old bird," Comput. Phys. Commun. **185**, 604–613 (2014).

[45]B. Roux, "The calculation of the potential of mean force using computer simulations," Comput. Phys. Commun. **91**, 275–282 (1995).

[46]F. Zhu and G. Hummer, "Convergence and error estimation in free energy calculations using the weighted histogram analysis method," J. Comput. Chem. **33**, 453–465 (2012).

[47]M. Sega, S. S. Kantorovich, P. Jedlovszky, and M. Jorge, "The generalized identification of truly interfacial molecules (itim) algorithm for nonplanar interfaces." J. Chem. Phys. **138**, 044110

(2013).

[48]L. B. Pártay, G. Hantal, P. Jedlovszky, A. Vincze, and G. Horvai, "A new method for determining the interfacial molecules and characterizing the surface roughness in computer simulations. Application to the liquid-vapor interface of water," J. Comput. Chem. **29**, 945–956 (2008).

[49]Y.-K. Cheng and P. J. Rossky, "Surface topography dependence of biomolecular hydrophobic hydration," Nature **392**, 696–699 (1998).

[50]P. N. Perera, K. R. Fega, C. Lawrence, E. J. Sundstrom, J. Tomlinson-Phillips, and D. Ben-Amotz, "Observation of water dangling OH bonds around dissolved nonpolar groups," Proc. Nat. Acad. Sci. U.S.A. **106**, 12230–12234 (2009).

[51]T. Ishiyama, H. Takahashi, and A. Morita, "Molecular dynamics simulations of surface-specific bonding of the hydrogen network of water: A solution to the low sum-frequency spectra," Phys. Rev. B **86** (2012).

[52]S. Ruiz-Barragan, D. Muñoz-Santiburcio, and D. Marx, "Nanoconfined water within graphene slit pores adopts distinct confinement-dependent regimes." J. Phys. Chem. Lett. **10**, 329–334 (2019).

[53]Y. Zhang, G. Stirnemann, J. T. Hynes, and D. Laage, "Water dynamics at electrified graphene interfaces: a jump model perspective," Phys. Chem. Chem. Phys. **22**, 10581 10591 (2020).

[54]Y. Zhang, H. B. de Aguiar, J. T. Hynes, and D. Laage, "Water structure, dynamics, and sum-frequency generation spectra at electrified graphene interfaces," J. Phys. Chem. Lett. **11**, 624–631 (2020).

[55]V. Subasinghege Don, R. David, P. Du, A. Milet, and R. Kumar, "Interfacial water at graphene oxide surface: Ordered or disordered," J. Phys. Chem. B **123**, 1636–1649 (2019).

[56]S. Xiao, F. Figge, G. Stirnemann, D. Laage, and J. A. McGuire, "Orientational Dynamics of Water at an Extended Hydrophobic Interface," J. Am. Chem. Soc. **138**, 5551–5560 (2016).

[57]F. Tang, T. Ohto, T. Hasegawa, W. J. Xie, L. Xu, M. Bonn, and Y. Nagata, "Definition of Free O-H Groups of Water at the Air-Water Interface," J. Chem. Theory Comput. **14**, 357–364 (2018).

[58]P. Jedlovszky, M. Předota, and I. Nezbeda, "Hydration of apolar solutes of varying size: a systematic study," Mol. Phys. **104**, 2465–2476 (2006).

[59]D. Matyushov, "Electrophoretic mobility of nanoparticles in water." J. Phys. Chem. B , in press (2024), doi.org/10.1021/acs.jpcb.3c08172.

[60]A. Graciaa, G. Morel, P. Saulner, J. Lachaise, and R. Schechter, "The ζ-potential of gas bubbles," J. Colloid. Interface. Sci. **172**, 131–136 (1995).

[61]S. Nihonyanagi, J. A. Mondal, S. Yamaguchi, and T. Tahara, "Structure and dynamics of interfacial water studied by heterodyne-detected vibrational sum-frequency generation." Annu. Rev. Phys. Chem. **64**, 579–603 (2013).

[62]H. B. de Aguiar, J.-S. Samson, and S. Roke, "Probing nanoscopic droplet interfaces in aqueous solution with vibrational sum-frequency scattering: A study of the effects of path length, droplet density and pulse energy," Chem. Phys. Lett. **512**, 76–80 (2011).

[63]R. Vácha, S. W. Rick, P. Jungwirth, A. G. F. de Beer, H. B. de Aguiar, J.-S. Samson, and S. Roke, "The Orientation and Charge of Water at the Hydrophobic Oil Droplet-Water Interface," J. Am. Chem. Soc. **133**, 10204–10210 (2011).

[64]S. M. Gruenbaum, C. J. Tainter, L. Shi, Y. Ni, and J. L. Skinner, "Robustness of frequency, transition dipole, and coupling maps for water vibrational spectroscopy," J. Chem. Theory Comput. **9**, 3109–3117 (2013).

[65]S. Iuchi, A. Morita, and S. Kato, "Molecular dynamics simulation with the charge response kernel: Vibrational spectra of liquid water and -methylacetamide in aqueous solution," J. Phys. Chem. B **106**, 3466–3476 (2002).

[66]T. Ohto, K. Usui, T. Hasegawa, M. Bonn, and Y. Nagata, "Toward ab initio molecular dynamics modeling for sum-frequency generation spectra; an efficient algorithm based on surface-specific velocity-velocity correlation function." J. Chem. Phys. **143**, 124702 (2015).

[67]G. Sommers, M. Calegari Andrade, L. Zhang, H. Wang, and R. Car, "Raman spectrum and polarizability of liquid water from deep neural networks." Phys. Chem. Chem. Phys. **22**, 10592–10602 (2020).

[68]M. de la Puente, A. Gomez, and D. Laage, "Neural network-based sum-frequency generation spectra of pure and acidified water interfaces with air," J. Phys. Chem. Lett. **15**, 3096–3102 (2024).

[69]B. Auer, R. Kumar, J. R. Schmidt, and J. L. Skinner, "Hydrogen bonding and Raman, IR, and 2D-IR spectroscopy of dilute HOD in liquid D2O," Proc. Natl. Acad. Sci. U.S.A. **104**, 14215–14220 (2007).

[70]S. Pullanchery, S. Kulik, B. Rehl, A. Hassanali, and S. Roke, "Charge transfer across C-H—O hydrogen bonds stabilizes oil droplets in water," Science **374**, 1366–1370 (2021).

[71]A. Gomez, Z. A. Piskulich, W. H. Thompson, and D. Laage, "Water Diffusion Proceeds via a Hydrogen-Bond Jump Exchange Mechanism," J. Phys. Chem. Lett. , 4660–4666 (2022).

[72]D. Laage and J. T. Hynes, "A Molecular Jump Mechanism of Water Reorientation," Science **311**, 832–835 (2006).

[73]G. Stirnemann, P. Rossky, J. Hynes, and D. Laage, "Water reorientation, hydrogen-bond dynamics and 2d-ir spectroscopy next to an extended hydrophobic surface." Faraday Discuss. **146**, 263–81 (2010).

[74]G. Stirnemann, S. R. Castrillón, J. T. Hynes, P. J. Rossky, P. G. Debenedetti, and D. Laage, "Non-monotonic dependence of water reorientation dynamics on surface hydrophilicity: competing effects of the hydration structure and hydrogen-bond strength." Phys. Chem. Chem. Phys. **13**, 19911–19917 (2011).

[75]P. Liu, E. Harder, and B. J. Berne, "On the Calculation of Diffusion Coefficients in Confined Fluids and Interfaces with an Application to the Liquid-Vapor Interface of Water," J. Phys. Chem. B **108**, 6595–6602 (2004).

[76]F. Pizzitutti, M. Marchi, F. Sterpone, and P. J. Rossky, "How protein surfaces induce anomalous dynamics of hydration water," J. Phys. Chem. B **111**, 7584–7590 (2007).

[77]B. Fábián, M. Sega, G. Horvai, and P. Jedlovszky, "Single Particle Dynamics at the Intrinsic Surface of Various Apolar, Aprotic Dipolar, and Hydrogen Bonding Liquids As Seen from Computer Simulations," J. Phys. Chem. B **121**, 5582–5594 (2017).

[78]H.-S. Tan, I. R. Piletic, and M. D. Fayer, "Orientational dynamics of water confined on a nanometer length scale in reverse micelles," J. Chem. Phys. **122**, 174501 (2005).

[79]Y. L. A. Rezus and H. J. Bakker, "On the orientational relaxation of HDO in liquid water," J. Chem. Phys. **123**, 114502 (2005).

[80]C. J. Fecko, J. J. Loparo, S. T. Roberts, and A. Tokmakoff, "Local hydrogen bonding dynamics and collective reorganization in water: Ultrafast infrared spectroscopy of HOD/D2O," J. Chem. Phys. **122**, 054506 (2005).

[81]D. Laage and J. T. Hynes, "On the Molecular Mechanism of Water Reorientation," J. Phys. Chem. B **112**, 14230–14242 (2008).

[82]A. Fogarty, E. Duboué-Dijon, F. Sterpone, J. Hynes, and D. Laage, "Biomolecular hydration dynamics: a jump model perspective." Chem. Soc. Rev. **42**, 5672–5683 (2013).

[83]E. Duboué-Dijon, A. Fogarty, J. Hynes, and D. Laage, "Dynamical disorder in the DNA hydration shell." J. Am. Chem. Soc. **138**, 7610–7620 (2016).

[84]D. Laage, G. Stirnemann, and J. T. Hynes, "Why Water Reorientation Slows without Iceberg Formation around Hydrophobic Solutes," J. Phys. Chem. B **113**, 2428–2435 (2009).

[85]P. Jungwirth and D. J. Tobias, "Ions at the air/water interface," J. Phys. Chem. B **106**, 6361–6373 (2002).

[86]Y. Marcus and G. Hefter, "Ion Pairing," Chem. Rev. **106**, 4585–4621 (2006).

[87]W. C. Duer, R. A. Robinson, and R. G. Bates, "Molar conductivity of sodium fluoride in aqueous solution at 25°C. applications of Pitts' conductivity equation," J. Chem. Soc., Faraday Trans. 1 **68**, 716–722 (1972).

[88]L. X. Dang, G. K. Schenter, and C. D. Wick, "Rate Theory of Ion Pairing at the Water Liquid-Vapor Interface," J. Phys. Chem. C **121**, 10018–10026 (2017).

[89]L. Fumagalli, A. Esfandiar, R. Fabregas, S. Hu, P. Ares, A. Janardanan, Q. Yang, B. Radha, T. Taniguchi, K. Watanabe, G. Gomila, K. S. Novoselov, and A. K. Geim, "Anomalously low dielectric constant of confined water," Science **360**, 1339–1342 (2018).

[90]S. Ruiz-Barragan, D. Muñoz-Santiburcio, S. Körning, and D. Marx, "Quantifying anisotropic dielectric response properties of nanoconfined water within graphene slit pores," Phys. Chem. Chem. Phys. **22**, 10833–10837 (2020).

[91]M. H. Motevaselian and N. R. Aluru, "Universal reduction in dielectric response of confined fluids," ACS Nano **14**, 12761–12770 (2020).

[92]J.-F. Olivieri, J. T. Hynes, and D. Laage, "Confined water's dielectric constant reduction is due to the surrounding low dielectric media and not to interfacial molecular ordering," J. Phys. Chem. Lett. **12**, 4319–4326 (2021).

[93]D. Borgis, D. Laage, L. Belloni, and G. Jeanmairet, "Dielectric response of confined water films from a classical density functional theory perspective," Chem. Sci. **14**, 11141–11150 (2023).

[94]R. Heyrovská, "Volumes of ions, ion pairs, and electrostriction of alkali halides in aqueous solutions at 25°C," Mar. Chem. **70**, 49–59 (2000).